Robust Security Analysis Based on Random Geometry Theory for Satellite-Terrestrial-Vehicle Network

Xudong Li, Ye Fan, Rugui Yao, *Senior Member, IEEE*, Peng Wang, Nan Qi, *Member, IEEE*, and Xiaoya Zuo, *Member, IEEE*

arXiv:2112.14192v1 [cs.IT] 28 Dec 2021

***Abstract*—Driven by *beyond fifth generation* (B5G) and *sixth generation* (6G) technologies, multi-network fusion is an indispensable tendency for future communications. In this paper, we focus on and analyze the *security performance* (SP) of the *satellite-terrestrial downlink transmission* (STDT). Here, the STDT is composed of a satellite network and a vehicular network with a legitimate mobile receiver and an mobile eavesdropper distributing. To theoretically analyze the SP of this system from the perspective of mobile terminals better, the random geometry theory is adopted, which assumes that both terrestrial vehicles are distributed stochastically in one beam of the satellite. Furthermore, based on this theory, the closed-form analytical expressions for two crucial and specific indicators in the STDT are derived, respectively, the secrecy outage probability and the ergodic secrecy capacity. Additionally, several related variables restricting the SP of the STDT are discussed, and specific schemes are presented to enhance the SP. Then, the asymptotic property is investigated in the high signal-to-noise ratio scenario, and accurate and asymptotic closed-form expressions are given. Finally, simulation results show that, under the precondition of guaranteeing the reliability of the STDT, the asymptotic solutions outperform the corresponding accurate results significantly in the effectiveness.**

***Index Terms*—Satellite-terrestrial downlink transmission, secrecy outage probability, ergodic secrecy capacity, random geometry theory, asymptotic analysis.**

I. Introduction

NOWADAYS, *satellite communication* (SatCom) applications with complete functions and mature systems get increasingly extensive due to accelerated scientific explorations and close connectivity. Meanwhile, the vehicular network has made remarkable progress in many aspects such as automatic drive, vehicular communication, and clean energy. Multi-network fusion idea and green communication viewpoint driven by *sixth generation* (6G) prompt satellite-terrestrial-vehicular communication to provide more convenience for information interaction. Nevertheless, the satellite deployment expansion is restricted inevitably as most SatComs adopt limited geosynchronous orbits and frequency resources. Accordingly, the current satellite-terrestrial-vehicular communication system is forced to suffer from a great deal of interference and malicious attacks in practice, which are considerably harmful to the security and stability of this system.

A. Literature Review

With technological development, SatCom security research is getting deeper and more specific. The *Communication Theory of Secrecy Systems* proposed by Claude Shannon in 1949 demonstrated that the confidential communication can be realized, when the transmitter and the legitimate receiver are always able to update secret keys each time [1]. Based on the aforementioned investigation, the theorem that the positive security capacity could only be achieved, when the noise power of the eavesdropping channel is greater than that of the authenticated receiver was illustrated by Wyner [2]. As related researches move along further, the model of the discrete memoryless eavesdropping channel was extended to the broadcasting channel and the Gaussian channel [3]. Some significant issues coming from the increasing demand of high-rate bands and low latency transmission of modern SatComs were analyzed and summarized in [4].

Then, the physical layer security in the SatCom has been closely focused, with the SatCom acting a increasingly key role. It is worth noting that more specific and further investigations on the SatCom secrecy performance were made with consideration of some techniques like the beamforming designing, the self-interference cancellation method, and the precoding algorithm. For example, several methods like the frequency domain non-orthogonal multiple access method and the self-interference cancellation method were presented, which could effectively improve the confidentiality performance in the SatCom in [5] and [6]. The authors of [7] suggested that for the sake of the enhancement of the SatCom networks security transmission, the base station equipped with multiple antennas can serve as a source of green interference. For preserving the security transmission, the authors of [8] proposed a random jamming scheme and a random precoding scheme, respectively, in the presence of a smart eavesdropper utilizing maximal likelihood detection. To minimize the total transmitting power of satellites, a successive convex approximation scheme was presented to convert the non-convex constraint into linear ones in [9]. A design of the secrecy radio frequency satellite links with the realistic system assumptions was presented, which demonstrated that the information theoretical secrecy

This work was supported in part by the National Natural Science Foundation of China (No.61701407, 61871327, and 61801218), in part by the Aerospace Science and Technology Fund of China under Grant 2020-HT-XG, and in part by the Shanghai Aerospace Science and Technology Innovation Fund under Grant SAST2019-078. *(Corresponding author: Rugui Yao.)*

Xudong Li, Ye Fan, Rugui Yao, Peng Wang, and Xiaoya Zuo are with the School of Electronics and Information, Northwestern Polytechnical University, Xi'an 710072, China (e-mail: xudong_good@mail.nwpu.edu.cn; fanye@nwpu.edu.cn; yaorg@nwpu.edu.cn; wangp126@mail.nwpu.edu.cn; zuoxy@nwpu.edu.cn).

Nan Qi is with the Key Laboratory of Dynamic Cognitive System of Electromagnetic Spectrum Space, Ministry of Industry and Information Technology, Nanjing University of Aeronautics and Astronautics, Nanjing 210016, China, and also with the National Mobile Communications Research Laboratory, Southeast University, Nanjing 210096, China (e-mail: nanqi.commun@gmail.com).

is a superior alternative to improve the secrecy performance in the SatCom [10]. To overcome the secrecy risk of the traditional secure constructive interference-based scheme when facing the smart eavesdroppers, a novel deception scheme via a random transmission strategy was presented in [11].

Remarkably, some literatures also further attach high significance to the *security performance* (SP) of satellite-terrestrial transmission, and derive several accurate analytical expressions of quantitative indices of the SP. Taking effects of the multibeam pattern and path loss into account, the *secrecy outage probability* (SOP) was derived in [12]. In the light of the scheduling scheme based on the adjustive threshold, the *closed-form analytical expressions* (CFAEs) of the SOP and *average secrecy capacity* (ASC) were attained in [13]. To evaluate the secrecy performance, the closed-form expressions of the SOP of each user, the overall SOP and the sum *effective secrecy throughput* (EST) of the considered FD-NOMA relay system are deduced [14]. To maximize the ASC and minimize the SOP of the SatCom, a novel beamforming designing technique was proposed in [15]-[18]. Then, with consideration of interference and malicious attacks resulting from eavesdroppers, robust beamforming schemes were presented to achieve the maximal ASC and the minimum SOP under eavesdropping in [19]-[21]. Some algorithms proposed recently were utilized to obtain the maximal value of the minimum ASC and SOP in [22] and [23].

However, to the best of authors' knowledge, random property of terrestrial terminals distribution and asymptotic property of security analyses are considered by few existing literatures. To sum up, existing investigations have attached inadequate significance to the influence, which is exerted by the randomness of positions of terrestrial terminals. Moreover, a lack of consideration of accurate calculated amount results in considerably negative effects on the practical engineering application of theoretical analyses.

B. Our Contributions

Motivated by the above research status, the *random geometry theory* (RGT) utilized and the *asymptotic analysis* (AA) proposed in this paper own remarkable advantages of approaching the reality scenario and enhancing the calculation efficiency.

Pointedly, the contributions of this paper are summarized as follows:

1) We derive the *probability density function* (PDF) and the *cumulative distribution function* (CDF) of the *received ratio of signal to noise* (RSNR) at terrestrial terminals via the RGT. Furthermore, we propose novel CFAEs of the SOP and the ESC based on the aforementioned random characterisitcs of terrestrial vehicles obtained in the presence of an eavesdropper in a satellite-terrestrial-vehicular communication scenario.
2) We present asymptotic expressions of the SOP and ESC in the high RSNR region with the consideration of that the series form of gamma function has an excellent approximation effect for the lower incomplete gamma function in the environment with the high RSNR based on Taylor series expansion method. Additionally, we provide a low-complexity analytical scheme for the SP of which the calculated efficiency is enhanced to 37% compared with accurate solutions.
3) We simulate accurate and asymptotic results of the SOP and the ESC, and then make a comparison with the numerical analysis on the theoretical analyses and simulation results. It shows that there exist optimal values for antenna numbers and fading parameter of the legitimate receiver for the enhancement of the effectiveness improvement.

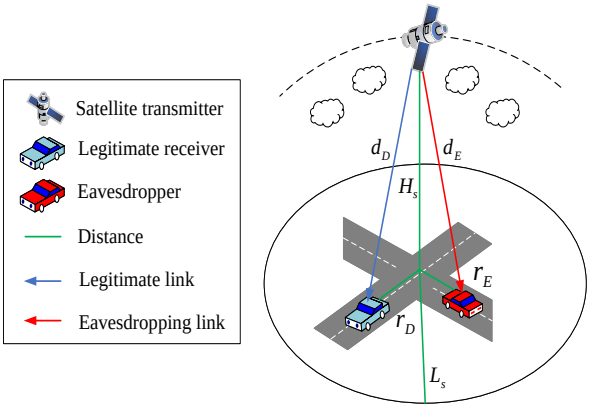

Fig. 1: System model of the STDT.

The remainder of this paper is organized as follows. Section II describes the STDT model. Then, the CDF and the PDF of the transmission gain and locations of vehicles are given, respectively, while the accurate and asymptotic CFAEs of the SOP are deduced in Section III. The statistical properties of the RSNR at terrestrial vehicles are derived and the accurate and asymptotic CFAEs of the ESC are obtained in Section IV. The numerical results and simulation analyses are presented in Section V. Finally, the last section concludes this paper.

II. System Model

In this section, the basic STDT model is illustrated, and then a parameter specification of the system structure, statistical characteristics of channel gains and the RSNRs at terrestrial terminals (i.e. vehicles) are given, respectively.

We consider a satellite-terrestrial downlink scenario, presented in Fig. 1, composed of a M_S-antennas satellite, two terrestrial terminals, namely a M_D-antennas legitimate receiver and a M_E-antennas unauthenticated eavesdropper. The satellite transmits security signals received by the legitimate receiver and the eavesdropper, when data transmission between the satellite and the legitimate receiver is necessary. Consequently, received signals at the receiver and the eavesdropper are modeled as:

$$y_D = P_S \mathbf{h}_{SD}^H \mathbf{x}_S + n, \tag{1a}$$

$$y_E = P_S \mathbf{h}_{SE}^H \mathbf{x}_S + n, \tag{1b}$$

where P_S, y_D and y_E denote the transmitting power, received signals at the receiver and the eavesdropper, respectively. $\mathbf{h}_{SD} \in {}^{M_S \times 1}$ and $\mathbf{h}_{SE} \in {}^{M_S \times 1}$ represent the channel

state information vector from the satellite to the receiver and the eavesdropper. $\mathbf{x}_S \in {}^{M_S\times 1}$ is security signal vector transmitted by the satellite, of which power is assumed to be 1. $n \in CN\left(0,\sigma^2\right)$ denotes additive complex random Gaussian noise at the receiver and the eavesdropper.

As is shown above, d_D and d_E are the distances from the satellite to the legal receiver and the illegal eavesdropper, respectively. H_S represents the vertical height of the satellite. r_D and r_E denote the distances from the center of the covered region by the satellite to the authenticated receiver and the illegal eavesdropper, respectively. The range on the ground of the satellite is a circular region of which radius is L_s. $\|\mathbf{h}_{sq}\|_2^2$ denotes the transmission gain of this downlink from the satellite to the terminal q. Additionally, the RSNR of the p_{th} antenna of the terminal q is $\gamma_{pq}=\frac{P_S|h_{pq}|^2}{\sigma^2 d_q^\tau}$. σ^2 is the average power of the additive white Gaussian noise (AWGN), $d_q = \left(r_q^2+H_s^2\right)^{1/2}$ is the distance from the satellite to the terminal q, r_q represents the distance between the center of the circular region and the terminal q, and τ denotes the path-loss factor of the downlink.

Moreover, this paper uses the Shadowed-Rician model proposed in [24] to obtain the statistical properties of the STDT, namely the CDFs and the PDFs of channel gains and the RSNRs at terrestrial terminals. Thus, the PDF of $|h_{pq}|^2$ is expressed as

$$f_{|h_{pq}|^2}(z) = \left(\frac{2\Delta_q\varepsilon_q}{2\Delta_q\varepsilon_q+\Omega_q}\right)^{\varepsilon_q}\frac{1}{2\Delta_q}e^{-z/2\Delta_q}\cdot {}_1F_1\left(\varepsilon_q,1,\frac{\Omega_q z}{2\Delta_q\left(2\Delta_q\varepsilon_q+\Omega_q\right)}\right), \quad (2)$$

where $p \in \{1,\cdots,M_q\}, q \in \{D,E\}$, Ω_q and $2\Delta_q$ are the average power of line-of-sight and scatter components. ε_q represents the fading severity parameter, and ${}_1F_1(\alpha,\gamma,z) = \sum_{n=0}^{\infty}\frac{1}{n!}\frac{(\alpha)_n}{(\gamma)_n}z^n$ denotes the first kind confluent hypergeometric function.

Let $\rho_{pq} = \frac{P_s}{\sigma^2}|h_{pq}|^2 = \bar{\gamma}|h_{pq}|^2$, where $\bar{\gamma} = \frac{P_S}{\sigma^2}$, and thus the PDF and CDF of ρ_{pq} are given by Eq. (3) and Eq. (4),

$$f_{\rho_{pq}}(z) = \alpha_q\sum_{k=0}^{\varepsilon_q-1}\frac{\zeta_q(k)}{\bar{\gamma}^{k+1}}z^k\exp\left(-\frac{\beta_q-\delta_q}{\bar{\gamma}}z\right), \quad (3)$$

$$F_{\rho_{pq}}(z) = 1-\alpha_q\sum_{k=0}^{\epsilon_q-1}\frac{\zeta_q(k)}{\bar{\gamma}^{k+1}}z^s\mathrm{e}^{\left(-\frac{\beta_q-\delta_q}{\bar{\gamma}}z\right)}A_4, \quad (4a)$$

$$A_4 = \sum_{s=0}^{k}z^s\mathrm{e}^{\left(-\frac{\beta_q-\delta_q}{\bar{\gamma}}z\right)}\frac{k!}{s!}\left(\frac{\beta_q-\delta_q}{\bar{\gamma}}\right)^{-(k+1-s)}, \quad (4b)$$

where $\alpha_q = \frac{\left(\frac{2\Delta_q\varepsilon_q}{2\Delta_q\varepsilon_q+\Omega_j}\right)^{\varepsilon_q}}{2\Delta_q}$, $\beta_q = \frac{1}{2\Delta_q}$, $\delta_q = \frac{\Omega_q}{2\Delta_q(2\Delta_q\varepsilon_q+\Omega_q)}$, and $\zeta_q(k) = \frac{(1-\varepsilon_q)_k(-\delta_q)^k}{(k!)^2}$.

Without loss of generality, it is assumed that the shape of this space is a right circular cone. Furthermore, statistical characteristics of both terrestrial vehicles are in uniform distribution. According to [26], the distances between two terrestrial vehicles and the projection of the satellite can be computed with the help of uniform distribution property κ, of which the PDF is given by $f_\kappa(z) = \pi^{-1}L_s^{-2}$. Based on the uniform distribution of terrestrial vehicles, the PDF and the CDF of r_q are expressed as

$$F_{r_q}(z) = \int_0^{2\pi}\int_0^z\frac{l}{\pi L_s^2}dld\theta = \frac{z^2}{L_s^2}, \quad (5a)$$

$$f_{r_q}(z) = \frac{\mathrm{d}F_{r_q}(z)}{\mathrm{d}z} = \frac{2z}{L_s^2}, l\in[0,L_s]. \quad (5b)$$

Consequently, on the strength of above derivations, the statistical characteristics of the distance from the satellite to terrestrial vehicles d_q^τ is given by

$$F_{d_q^\tau}(z) = F_{r_q}\left(\left(z^{2/\tau}-H_S^2\right)^{1/2}\right) = \frac{z^{2/\tau}-H_S^2}{L_S^2}, \quad (6a)$$

$$f_{d_q^\tau}(z) = \frac{\mathrm{d}F_{d_q^\tau}(z)}{\mathrm{d}z} = \frac{2z^{2/\tau-1}}{\tau L_S^2}, \quad (6b)$$

which indicates that the randomness of the two-dimension terrestrial-vehicular network is introduced into the three-dimension satellite-terrestrial-vehicular network naturally. With the characteristic of the maximal ratio combining considered, the RSNR at terminal q is represented as

$$\gamma_q = \sum_{a=0}^{M_q}\gamma_{aq} = \sum_{a=0}^{M_q}\frac{\rho_{aq}}{d_q^\tau} = \frac{\sum_{a=0}^{M_q}\rho_{aq}}{d_q^\tau} = \frac{\rho_q}{d_q^\tau}. \quad (7)$$

On the account of aforementioned investigations, the accurate and asymptotic solutions of $\mathrm{P_r}$ and $\bar{C}_S$ are given to evaluate the SP of the STDT better via the RGT and the AA in Section III and Section IV.

III. Analysis of the SOP

In this section, the analytical solutions of the accurate and asymptotic SOPs defined as that the probability of the secrecy capacity is less than 0 are obtained.

In the light of [25], the PDF of ρ_q is given by

$$f_{\rho_q}(z) = \left(\frac{2\Delta_q\varepsilon_q}{2\Delta_q\varepsilon_q+\Omega_q}\right)^{\tilde{\varepsilon}_q}\frac{z^{M_q-1}\exp\left(-\frac{z}{2\Delta_q\bar{\gamma}}\right)}{\Gamma(M_q)(2\Delta_q)^{M_q}\bar{\gamma}^{M_q}}A_8, \quad (8a)$$

$$A_8 = {}_1F_1\left(\tilde{\varepsilon}_q,M_q,\frac{\Omega_q z}{2\Delta_q\left(2\Delta_q\varepsilon_q+\Omega_q\right)\bar{\gamma}}\right), \quad (8b)$$

where $\Gamma(z) = \int_0^\infty t^{z-1}e^{-t}dt$ denotes the complete gamma function. With the computation complexity of the first kind confluent hypergeometric function considered, Eq. (8) is rewritten as [27]

$$f_{\rho_q}(z) = \frac{\tilde{\alpha}_q}{\tilde{\beta}_q}\sum_{k=0}^{\tilde{\varepsilon}_q-M_q}\theta_{qk}\exp\left(-\psi_q z\right)z^{k+M_q-1}, \quad (9)$$

where $\tilde{\alpha}_q = \left(\frac{2\Delta_q\varepsilon_q}{2\Delta_q\varepsilon_q+\Omega_q}\right)^{\tilde{\varepsilon}_q}$, $\tilde{\beta}_q = \Gamma(M_q)(2\Delta_q)^{M_q}\bar{\gamma}^{M_q}$, $\tilde{\sigma}_q = \frac{\Omega_q}{2\Delta_q(2\Delta_q\varepsilon_q+\Omega_q)\bar{\gamma}}$, $\theta_{qk} = \frac{(\tilde{\varepsilon}_q-M_q)!\tilde{\sigma}_q^k}{k!(\tilde{\varepsilon}_q-M_q-k)!(M_q)_k}$, and $\psi_q = \frac{1}{2\Delta_q\bar{\gamma}}-\tilde{\sigma}_q$.

Thus, the CDF of ρ_q is obtained as Eq. (10),

$$F_{\rho_q}(z) = 1 - \frac{\tilde{\alpha}_q}{\tilde{\beta}_q} \sum_{k=0}^{\tilde{\varepsilon}_q - M_q} \theta_{qk} \sum_{s=0}^{k+M_q-1} \tilde{\zeta}_{ks} z^s \exp(-\psi_q z) \psi_q^m, \tag{10}$$

where $\tilde{\zeta}_{ks} = \frac{(k+M_q-1)!}{s!}$, and $m = -(k+M_q-s)$. The secrecy capacity of the STDT is defined as the difference between the secrecy capacity of the legitimate receiver and that of the eavesdropper, namely

$$C_S(\gamma_D, \gamma_E) = \left(\log_2 \frac{1+\gamma_D}{1+\gamma_E}\right)^+, \tag{11}$$

where $(z)^+ = \max(z, 0)$, γ_D and γ_E denote the total RSNRs at the receiver and the eavesdropper, respectively. The outage event means the confidentiality capacity is negative, based on which the SOP is represented as

$$\mathrm{P_r} = \mathrm{P_r}\{C_S(\gamma_D, \gamma_E) \le 0\}. \tag{12}$$

The subsequent theoretical analyses of the SOP and the ESC are derived, with the above statistical properties of the RSNRs at the legitimate receiver and the unauthenticated eavesdropper, as well as the definitions of the secrecy capacity and the secrecy outage event considered. Then, the specific deduction process of the SOP is given as follows.

A. Accurate Analysis of the SOP

1) CFAE without randomness of terminals: The non-CFAE of the SOP without randomness is expressed as

$$\mathrm{P_{r|}}_{d_D, d_E} = 1 - \int_0^\infty \sum_{k=0}^{\tilde{\varepsilon}_D - M_D} \sum_{t=0}^{k+M_D-l} \sum_{l=0}^{\tilde{\varepsilon}_E - M_E} \Lambda_{k,t,l} A_{13} dz \ , \tag{13a}$$

$$A_{13} = \left(\frac{d_D^\tau}{d_E^\tau}\right)^t \exp\left[-\left(\psi_D \frac{d_D^\tau}{d_E^\tau} + \psi_E\right) z\right] z^{l+t+M_E-1}. \tag{13b}$$

According to [28], the integral part of Eq. (13) can be substituted by

$$\int_0^\infty \sum_{k=0}^{\tilde{\varepsilon}_D - M_D} \sum_{t=0}^{k+M_D-l} \sum_{l=0}^{\tilde{\varepsilon}_E - M_E} \Lambda_{k,t,l} A_{14} dz = \sum_{k,t,l} \Lambda_{k,t,l} B_{14}, \tag{14a}$$

$$A_{14} = \left(\frac{d_D^\tau}{d_E^\tau}\right)^t \exp\left[-\left(\psi_D \frac{d_D^\tau}{d_E^\tau} + \psi_E\right) z\right] z^{l+t+M_E-1}, \tag{14b}$$

$$B_{14} = \left(\frac{d_D^\tau}{d_E^\tau}\right)^t \frac{\Gamma(l+t+M_E)}{\left(\psi_D \frac{d_D^\tau}{d_E^\tau} + \psi_E\right)^{l+t+M_E}}. \tag{14c}$$

Here, by substituting Eq. (14) into Eq. (13), the accurate CFAE without randomness can be expressed as

$$\mathrm{P_{r|}}_{d_D, d_E} = 1 - \sum_{k,t,l} \Lambda_{k,t,l} \left(\frac{d_D^\tau}{d_E^\tau}\right)^t \frac{\Gamma(l+t+M_E)}{\left(\psi_D \frac{d_D^\tau}{d_E^\tau} + \psi_E\right)^{l+t+M_E}}, \tag{15}$$

where $\Lambda_{k,t,l} = \frac{\tilde{\alpha}_D \tilde{\alpha}_E \theta_{Dk} \theta_{El} \tilde{\zeta}_{kt}}{\tilde{\beta}_D \tilde{\beta}_E \psi_D^{k+A-t}}$.

2) CFAE with randomness of terminals: By adopting Eq. (15), with randomness of two terminals, the non-CFAE of the SOP is given in Eq. (16),

$$\mathrm{P_r} = 1 - \sum_{k,t,l} \Lambda_{k,t,l} \frac{4\Gamma(l+t+M_E)}{\tau^2 L_s^4} A_{16}, \tag{16a}$$

$$A_{16} = \int_{d_{\min^\tau}}^{d_{\max^\tau}} \int_{d_{\min^\tau}}^{d_{\max^\tau}} \frac{z_D^{2\tau^{-1}+t-1} z_E^{l+M_E+2\tau^{-1}-1}}{(\psi_D z_D + \psi_E z_E)^{l+t+M_E}} dz_D dz_E, \tag{16b}$$

where $d_{\min} = H_s$ and $d_{\max} = \sqrt{H_s^2 + L_s^2}$. The integral part of the non-CFAE with considering the randomness (i.e. Eq. (16)) can be substituted by Eq. (17) [30],

$$\begin{aligned} &\int_{d_{\min}^\tau}^{d_{\max}^\tau} \frac{z_d^{\frac{2}{\tau}+t-1}}{(\psi_D z_d + \psi_E z_e)^{l+t+M_E}} dz_d = \\ &\frac{(d_{\min}^\tau)^{-\mu_l}}{\mu_l \psi_D^{\nu_{pl}}} {}_2F_1\left(\nu_{pl}, \mu_l; 1+\mu_l, -\frac{\psi_E z_e}{\psi_D d_{\min}^\tau}\right) - \\ &\frac{(d_{\max}^\tau)^{-\mu_l}}{\mu_l \psi_D^{\nu_{pl}}} {}_2F_1\left(\nu_{pl}, \mu_l; 1+\mu_l, -\frac{\psi_E z_e}{\psi_D d_{\max}^\tau}\right), \end{aligned} \tag{17}$$

where $v_{lt} = l + t + M_E$ and $u_l = l - \frac{2}{\tau} + M_E$. By substituting Eq. (17) into Eq. (16), Eq. (16) can be deduced into Eq. (18),

$$\begin{aligned} &\mathrm{P_r} = 1 - \\ &\sum_{k,t,l} \Lambda_{k,t,l} \frac{4\Gamma(l+t+M_E)}{\tau^2 L_s^4} \int_{d_{\min}^\tau}^{d_{\max}^\tau} z_e^{l+M_E+\frac{2}{\tau}-1} \frac{(d_{\min}^\tau)^{-\mu_l}}{\mu_l \psi_D^{\nu_{tl}}} * \\ &{}_2F_1\left(\nu_{tl}, \mu_l; 1+\mu_l, -\frac{\psi_E z_e}{\psi_D d_{\min}^\tau}\right) dz_e + \\ &\sum_{k,t,l} \Lambda_{k,t,l} \frac{4\Gamma(l+t+M_E)}{\tau^2 L_s^4} \int_{d_{\min}^\tau}^{d_{\max}^\tau} z_e^{l+M_E+\frac{2}{\tau}-1} \frac{(d_{\max}^\tau)^{-\mu_l}}{\mu_l \psi_D^{\nu_{tl}}} * \\ &{}_2F_1\left(\nu_{tl}, \mu_l; 1+\mu_l, -\frac{\psi_E z_e}{\psi_D d_{\max}^\tau}\right) dz_e, \end{aligned} \tag{18}$$

where ${}_2F_1(\alpha, \gamma, z)$ represents the hypergeometric function. Herein, Meijers G-function is utilized to denote this function, and $g(a, b, c, d)$ is introduced in [29], which is rewritten as Eq. (19),

$$g(a, b, c, d) = \frac{\Gamma(1+\mu_c)}{\Gamma(\nu_{dc})\Gamma(\mu_c)} a^{\eta_c+1} A_{19}, \tag{19a}$$

$$A_{19} = G_{3,3}^{1,3}\left[ba \middle| \begin{matrix} 1-\nu_{dc} & 1-\mu_c & -\eta_c \\ 0 & -1-\eta_c & -\mu_c \end{matrix}\right]. \tag{19b}$$

By employing Eq. (19), Eq. (18) (i.e. accurate non-CFAE with randomness of the SOP) can be deduced into Eq. (20),

$$\begin{aligned} &\mathrm{P_r} = 1 - \\ &\sum_{k,t,l} \Lambda_{k,t,l} \frac{4\Gamma(l+t+M_E)}{\tau^2 L_s^4} \frac{(d_{\min}^\tau)^{-\mu_l}}{\mu_l \psi_D^{\nu_{tl}}} * \\ &\left[g\left(d_{\max}^\tau, \frac{\psi_E}{\psi_D d_{\min}^\tau}, l, t\right) - g\left(d_{\min}^\tau, \frac{\psi_E}{\psi_D d_{\min}^\tau}, l, t\right)\right] + \\ &\sum_{k,t,l} \Lambda_{k,t,l} \frac{4\Gamma(l+t+M_E)}{\tau^2 L_s^4} \frac{(d_{\max}^\tau)^{-\mu_l}}{\mu_l \psi_D^{\nu_{tl}}} * \\ &\left[g\left(d_{\max}^\tau, \frac{\psi_E}{\psi_D d_{\max}^\tau}, l, t\right) - g\left(d_{\min}^\tau, \frac{\psi_E}{\psi_D d_{\max}^\tau}, l, t\right)\right]. \end{aligned} \tag{20}$$

The analysis of the accurate CFAE of the SOP are introduced and derived at the above subsection. Obviously, plenty of calculated amount is involved in this process, which urges us to search for an effective scheme to obtain analytical solutions close to the above resluts. Hence, the AA to achieve this effect is proposed.

B. Asymptotic Analysis of the SOP

Doubtlessly, the calculation complexity involved in the accurate CFAE of the SOP in Eq. (20) makes it inconvenient be applied into the practical scenario due to considerable calculated amount. Considering such a disadvantage, the AA is a reasonable alternative in the study of the high RSNR area, which is regarded as an effective reference for designing the layout of the STDT.

The CDF of ρ_q is given by [25]

$$F_{\rho_q}(z) = \frac{\tilde{\alpha}_q}{\tilde{\beta}_q} \sum_{k=0}^{\tilde{\varepsilon}_q - M_q} \theta_{qk} \frac{\gamma(k + M_q, \psi_q z)}{\psi_q^{k+M_q}}, \tag{21}$$

where $\gamma(s,z) = \int_0^z t^{s-1} e^{-t} dt$ represents the lower incomplete gamma function. Accordingly, in the light of [30], this gamma function can be expressed as in the high RSNR area scenario,

$$\gamma(\alpha, z) = \sum_{n=0}^{\infty} \frac{(-1)^n z^{(\alpha+n)}}{n!(\alpha+n)}, \tag{22}$$

and then the asymptotic CDF of ρ_q is expressed as

$$F_{\rho_q}^{\infty}(z) = \frac{\tilde{\alpha}_q}{\tilde{\beta}_q} \sum_{k=0}^{\tilde{\varepsilon}_q - M_q} \theta_{qk} \frac{(\psi_q z)^{k+M_q}}{(k+M_q)\psi_q^{k+M_q}}. \tag{23}$$

Based on [30], the CFAE without considering randomness is given by

$$\mathrm{P}_{\mathrm{r}|d_D,d_E}^{\infty} = \sum_{k=0}^{\tilde{\varepsilon}_D - M_D} \sum_{l=0}^{\tilde{\varepsilon}_E - M_E} o_{kl} \left(\frac{d_D}{d_E}\right)^{\tau(k+M_D)}, \tag{24}$$

where $o_{kl} = \frac{\tilde{\alpha}_D \tilde{\alpha}_E \theta_{Dk} \theta_{El} \Gamma(k+l+M_D+M_E)}{\tilde{\beta}_D \tilde{\beta}_E (k+M_D) \psi_E^{2k+M_D+M_E}}$. Consequently, with the randomness of two terminals considered, the asymptotic CFAE of the SOP is represented as

$$\begin{aligned} \mathrm{P}_{\mathrm{r}}^{\infty} = & \tfrac{4}{\tau^2 L_s^4} \sum_{k=0}^{\tilde{\varepsilon}_D - M_D} \sum_{l=0}^{\tilde{\varepsilon}_E - M_E} \cdot \\ & \frac{\tilde{\alpha}_D \tilde{\alpha}_E \theta_{Dk} \theta_{El} \Gamma(k+l+M_D+M_E)}{\tilde{\beta}_D \tilde{\beta}_E (k+M_D) \psi_E^{2k+M_D+M_E}} \cdot \\ & \left(\frac{d_{\max}^{\tau(k+M_D)+2}}{\frac{2}{\tau}+k+M_D} - \frac{d_{\min}^{\tau(k+M_D)+2}}{\frac{2}{\tau}+k+M_D} \right) \cdot \\ & \left(\frac{d_{\max}^{2-\tau(k+M_D)}}{\frac{2}{\tau}-k-M_D} - \frac{d_{\min}^{2-\tau(k+M_D)}}{\frac{2}{\tau}-k-M_D} \right). \end{aligned} \tag{25}$$

Compared with the accurate CFAE of the SOP, the complicated mathematical computation of the asymptotic one is reduced significantly, with the gamma function substituted via the series representation. In addition, the advantage of the AA will be further validated via the Monte Carlo simulation in the Section V.

IV. Analysis of the ESC

In this section, the PDF and CDF of γ_q are deduced, and then the accurate and asymptotic CFAEs of the ESC are derived.

The ESC is defined as the statistical average value of confidentiality capacities, namely

$$\bar{C}_S = \int_0^{\gamma_D} \int_0^{\gamma_E} \log_2 \frac{1+\gamma_D}{1+\gamma_E} f_{\Upsilon_D}(\gamma_D) f_{\Upsilon_E}(\gamma_E) d\gamma_D d\gamma_E. \tag{26}$$

According to Section II, with maximal ratio combining technique adopted, the total RSNR at terrestrial terminal q is expressed as $\gamma_q = \rho_q / d_q^{\tau}$. For the sake of brevity, it is defined as

$$x = \gamma_D, y = \gamma_E. \tag{27}$$

Thereby, Eq. (26) can be rewritten as

$$\bar{C}_S = \int_0^x \int_0^y \log_2 \frac{1+x}{1+y} f_{X,Y}(x,y) dx dy. \tag{28}$$

In addition, the statistical characteristics of two terrestrial terminals are mutually independent, namely

$$\begin{aligned} & \bar{C}_S = \\ & F_Y(y)|_0^y \int_0^x f_X(x) \log_2(1+x) dx - \\ & F_X(x)|_0^x \int_0^y f_Y(y) \log_2(1+y) dy. \end{aligned} \tag{29}$$

By employing Eq. (7), the relationship between the CDF of γ_q and that of ρ_q is denoted by

$$F_{\gamma_q}(t) = F_{\rho_q}\left(d_q^{\tau} t\right). \tag{30}$$

Then, by substituting Eq. (9) and Eq. (23) into Eq. (30), the accurate and asymptotic CDFs of the RSNR at the receiver and the eavesdropper are represented as Eq. (31) and Eq. (32), respectively,

$$F_{\gamma_q}(z) = 1 - \frac{\tilde{\alpha}_q}{\tilde{\beta}_q} \sum_{k=0}^{\tilde{\varepsilon}_q - M_q} \theta_{qk} \sum_{t=0}^{k+M_q-1} A_{31}, \tag{31a}$$

$$A_{31} = \tilde{\varsigma}_{kt} \psi_q^{-(k+M_q-t)} \left(d_q^{\tau} z\right)^t \exp\left(-\psi_q d_q^{\tau} z\right), \tag{31b}$$

$$F_{\gamma_q}^{\infty}(z) = \frac{\tilde{\alpha}_q}{\tilde{\beta}_q} \sum_{k=0}^{\tilde{\varepsilon}_q - M_q} \theta_{qk} \frac{\left(d_q^{\tau} z\right)^{k+M_q}}{(k+M_q)}. \tag{32}$$

Consequently, by differentiating the CDFs above, the accurate and asymptotic PDFs are expressed as Eq. (33) and Eq. (34), respectively,

$$f_{\gamma_q}(z) = d_q^{\tau} \frac{\tilde{\alpha}_q}{\tilde{\beta}_q} \sum_{k=0}^{\tilde{\varepsilon}_q - M_q} \theta_{qk} e^{-\psi_q d_q^{\tau} z} \left(d_q^n z\right)^{k+M_q-1}, \tag{33}$$

$$f_{\gamma_q}^{\infty}(z) = \frac{\tilde{\alpha}_q}{\tilde{\beta}_q} \sum_{k=0}^{\tilde{\varepsilon}_q - M_q} \theta_{qk} \left(d_q^{\tau}\right)^{k+M_q} t^{k+M_q-1}. \tag{34}$$

Based on the aforementioned results, the accurate and aymptotic ESCs without containing the randomness are represented

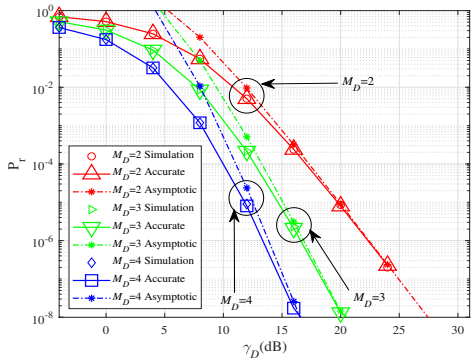

(a) SOP versus γ_D for different M_D.

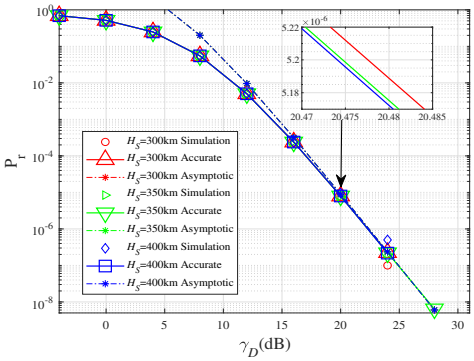

(b) SOP versus γ_D for different H_S.

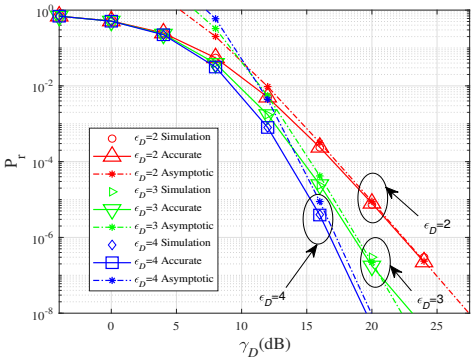

(c) SOP versus γ_D for different ϵ_D.

Fig. 2: SOP versus γ_D for different related variables.

as Eq. (35) and Eq. (36), respectively, please see the Appendix A.

By swapping the order of integration and sum, and adopting equations in [30], Eq. (35) and Eq. (36) can be rewritten as Eq. (37) and Eq. (38). Then, the accurate CFAE with randomness of the ESC is expressed as Eq. (39). In a simialr way, the asymptotic CFAE is obtained as Eq. (40). Specific equations are displayed in Appendix A.

Different from Section III, here, the intuitive computation variance between the accurate and the asymptotic CFAEs of the ESC is not remarkable. Hence, in the next section, by means of the Monte Carlo simulation, the calculation complexities of the accurate and asymptotic results are compared, and the above difference is further given exactly.

TABLE I: Downlink Transmission Parameters.

Parameter	Value
Radius of circle (L_s)	15km
Receiving SNR at receiver (γ_D)	30dB
Receiving SNR at eavesdropper (γ_E)	10dB
Fading severity parameter of S-R (ε_D)	2
Fading severity parameter of S-E (ε_E)	2
Average power of scatter components ($2\Delta_D$)	0.72
Average power of scatter components ($2\Delta_E$)	0.5
Path-loss factor (τ)	2

V. Numerical Results and Simulation Analyses

In this section, accurate and asymptotic results of SOP and ESC are simulated via Monte Carlo simulation. Then, theoretical analyses and simulation results are compared to confirm the reliability of the STDT model and methods presented in this paper.

A. Analysis of the Single Variable

1) SOP versus γ_D for different M_D: The γ_D versus $\mathrm{P_r}$ for different values of M_D is shown in Fig. 2(a). As can be seen, there are some variances shown in Fig. 2(a). Here, the greater the value of γ_D is, the less that of $\mathrm{P_r}$ is, which makes a contribution to a more excellent SP improvement. With such a phenomenon noted, there exist two perspectives to explain this result. On the one hand, $\mathrm{P_{r|}}_{d_D,d_E}{}'(\gamma_D) < 0$ indicates that with greater RSNR at the receiver obtained, the SP is getting better. On the other hand, since a better satellite-receiver channel quality can be provided by a higher γ_D, which strengthens the ability of the system to withstand eavesdropping risks. Meanwhile, at the same value of γ_D, the SOP decreases, with M_D improving. In addition, the asymptotic result is so closed to the accurate one that differences between them can be neglected in the high RSNR region scenario. Since the series representations of gamma function have a brilliant substitute effect on the original gamma function, when values involved in it are much greater.

2) SOP versus γ_D for different M_D: The H_S versus $\mathrm{P_r}$ for various values of H_S is shown in Fig. 2(b), where some variances are described. Herein, the change of H_s has a negligible effect on the SOP. Herein, the distance from the satellite to the terrestrial terminal q is defined as $d_q = \sqrt{H_s^2 + r_q^2} \approx H_s$, when the value of H_s is much greater than r_D and r_E. What's more, this results in an approximately identical effect on two terrestrial terminals, when the height of the satellite is fluctuating, which explains that the SP of the STDT is not influenced remarkably by H_s.

3) SOP versus γ_D for different ϵ_D: The γ_D versus $\mathrm{P_r}$ for different values of ε_D is shown in Fig. 2(c). Here, at the same value of γ_D, the SOP decreases when ε_D is improving. In the light of Eq. (14), with ε_D increasing, $\tilde{\varepsilon}_D = \sum_{p=0}^{A_D} \varepsilon_D = M_D \varepsilon_D$ also increases, thus the integral part improves. Then, $\mathrm{P_{r|}}_{d_D,d_E}$ decreases, and the SP gets better, which has been validated via numerical results.

4) ESC versus γ_D for different M_D: The γ_D versus $\bar{C}_S$ for various values of M_D is shown in Fig. 3(a). Here, the greater the value of γ_D is, the greater that of $\bar{C}_S$ is

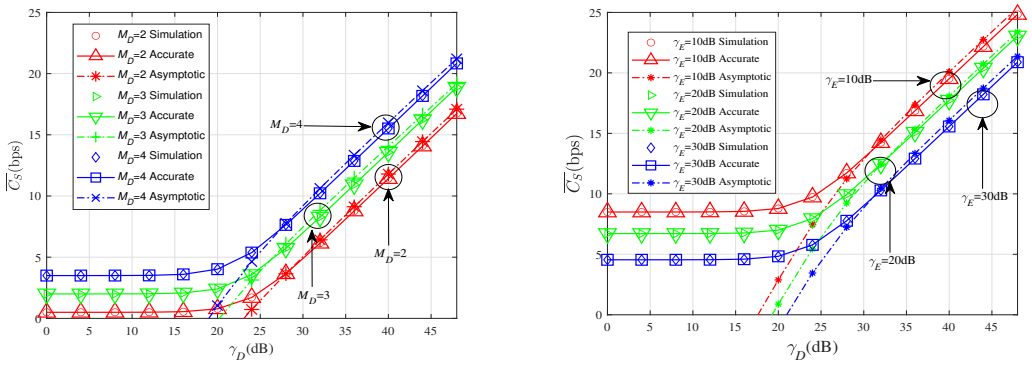

(a) ESC versus γ_D for different M_D. (b) ESC versus γ_D for different γ_E.

Fig. 3: ESC versus γ_D for different related variables.

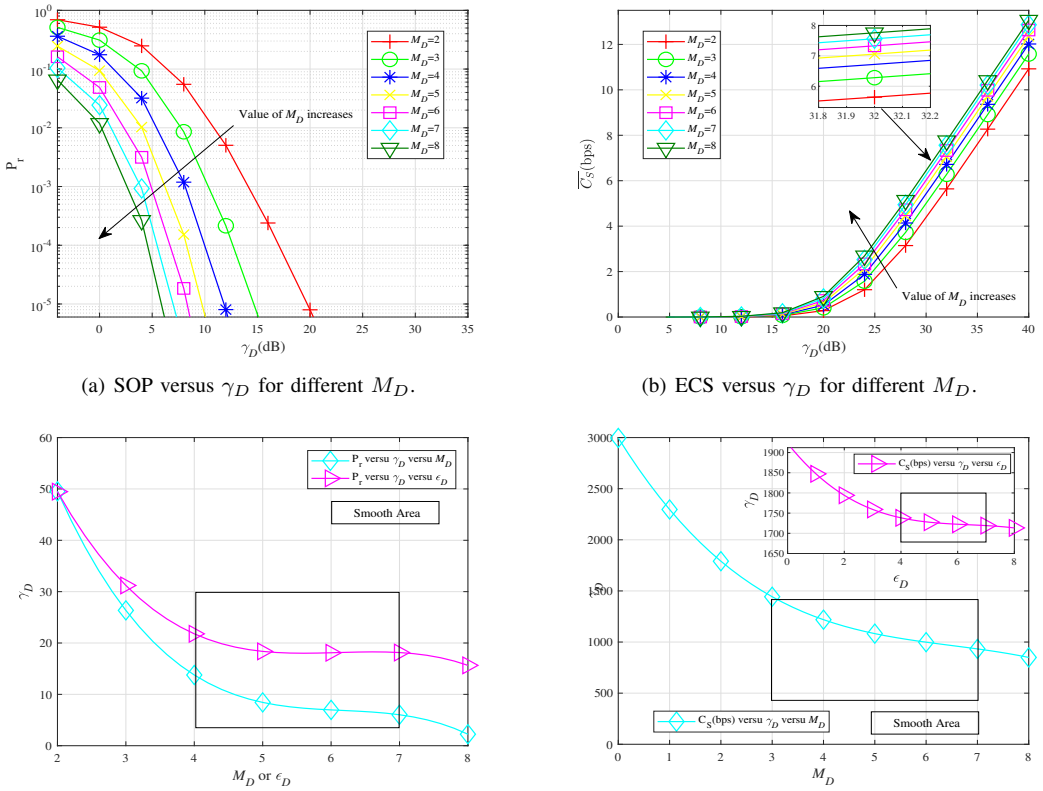

(a) SOP versus γ_D for different M_D. (b) ECS versus γ_D for different M_D.

(c) Fitted curve of different γ_D versu M_D and ϵ_D for $\mathrm{P_r}$. (d) Fitted curve of different γ_D versu M_D and ϵ_D for $\bar{C}_S$.

Fig. 4: Parameter optimization analysis of the STDT.

implemented, which makes a contribution to a more excellent SP achieved. With such a phenomenon considered, there exist two perspectives to understand this result. On the one hand, $\bar{C}'_{S|d_D,d_E}(\gamma_D) > 0$ means the greater value of γ_D is, the greater those of $\bar{C}_{S|d_D,d_E}$ and $\bar{C}_S$ are. On the other hand, $\bar{C}_S$ increases when γ_D improves. This is rational because a higher γ_D can provide a better quality of downlink transmission, which prompt a superior strength to preserve the secrecy datas from eavesdropping. Accordingly, more secrecy signals are transmitted, which implies a greater security capacity is fulfilled. Besides, for a fixed γ_D, a improved M_D can prompt the enhancement of the $\bar{C}_S$. Since the maximal ratio combining technology is adopted, by which a better received diversity gain is attained via more antennas at the receiver. A superior satellite-receiver channel quality thereby can be provided, which assures a greater value of $\bar{C}_S$ and a better SP of the STDT.

5) ESC versus γ_D for different γ_E: The γ_D versu $\bar{C}_S$ for different values of γ_E is shown in Fig. 3(b), which displays that at the same value of γ_D, $\bar{C}_S$ decreases when γ_E is improving. Because an increasing γ_E leads to more anti-eavesdropping overhead, which results in a worse performance

TABLE II: Comparison of the effectiveness and the reliability.

	Item	Time Complication		Computation Accuracy	
		$\mathrm{P_r}$	$\bar{C}_S$	$\mathrm{P_r}$	$\bar{C}_S$
Case 1: H_S=300km	Asymptotic	465.668seconds	565.428seconds	2.306×10^{-7}	18.61bps
	Accurate	732.047seconds	886.960seconds	2.254×10^{-7}	18.18bps
	Improved	$+36.388\%$	$+36.251\%$	-2.303%	-2.365%
Case 2: H_S=350km	Asymptotic	457.351seconds	562.020seconds	2.260×10^{-7}	18.62bps
	Accurate	732.372seconds	891.289seconds	2.206×10^{-7}	18.23bps
	Improved	$+37.552\%$	$+36.943\%$	-2.449%	-2.139%
Case 3: H_S=400km	Asymptotic	458.080seconds	553.337seconds	2.231×10^{-7}	18.45bps
	Accurate	740.051seconds	880.774seconds	2.174×10^{-7}	18.08bps
	Improved	$+38.102\%$	$+37.176\%$	-2.607%	-2.046%

of the STDT. Then, $\bar{C}_S$ decreases proportionally.

B. Analysis of the Multi-parameter Optimization

For the sake of showing the effects clearly and simply, here accurate expressions are adopted, and simulation and asymptotic ones are omitted. With consideration of that influences exerted via ϵ_D and M_D are similar, figures reflecting effects of ϵ_D are omitted, too. Fig. 2 and Fig. 3 have demonstrated that the SP of the STDT gets improved with greater values of M_D and ϵ_D. However, it is found that there exists a tendency that the growth of improvement of the SP is subject to slowing down, when more experiments are cunducted. This condition encourages us to invesgate more as displayed in Fig. 4(a) and Fig. 4(b).

1) SOP versus γ_D for different M_D: The γ_D versus $\mathrm{P_r}$ for different values of M_D is shown in Fig. 4(a). As can be observed, the enhancement of improvement of $\mathrm{P_r}$ is slowing down indeed. Take $\mathrm{P_r} = 10^{-4}$, for example. For achieving this SP, the RSNRs at the legitimate receiver needed are 50.093, 18.406, 9.841, 6.699, 4.657, 3.510, and 2.840, when values of M_D are 2, 3, 4, 5, 6, 7, and 8, respectively. Moreover, take $M_D = 2$ as a baseline. Then, improvements of P_{r} obtained are 63.256%, 80.355%, 86.627%, 90.703%, 92.993%, and 94.331%, which implies the difference values between the adjoining items are 17.099%, 6.272%, 4.076%, 2.290%, and 1.338%, respectively.

2) ESC versus γ_D for different M_D: In a similar way, Fig. 4(b) depicts the γ_D versus $\bar{C}_S$ for various values of M_D. As can be seen, the enhancement of improvement of $\mathrm{P_r}$ is also slowing down. Take $\bar{C}_S = 10\mathrm{bps}$, for example, with $M_D = 2$ deemed as a baseline still. To get the same SP, the RSNRs at the legitimate receiver needed are 7278.804, 5751.750, 4962.951, 4413.570, 3993.006, 3718.262, and 3431.863, when values of M_D are 2, 3, 4, 5, 6, 7, and 8, respectively. The improvements of $\bar{C}_S$ attained are 20.979%, 31.816%, 39.364%, 45.142%, 48.917%, and 52.851%, which indicates the difference values between the adjoining items are 10.837%, 7.548%, 5.778%, 3.934%, and 3.755%, respectively.

3) fitted curve of different γ_D versu M_D and ϵ_D for $\mathrm{P_r}$ and $\bar{C}_S$: These numerical results illustrate that the above analyses are reasonable. To observe these variances intuitively, fitted curves are made as displayed in Fig. 4(c) and Fig. 4(d), where successive variances of improvements of $\mathrm{P_r}$ and $\bar{C}_S$ affected via M_D and ϵ_D are shown, respectively. Based on these figures, a better enhancement of improvement of the SP is attained, especially considering the antenna interference issue and the complexity of designing. Accordingly, an excellent scheme can be achieved where optimal values of M_D and ϵ_D are 5 and 5, respectively.

C. Analysis of the Improvements of the Effectiveness and the Reliability

The variances associated with the calculation complexity measured by run time for programs (i.e. effectiveness) and the computation accuracy measured via margins of error between accurate and asymptotic solutions (i.e. reliability) are displayed in TABLE II. Therefore, variances are discussed from two demonsions as below:

1) From the Point of Horizontal Direction: With the similarity of the variance tendency in the horizontal direction considered, take the Case 1 as an example to illustrate the specific advantage of the AA. Compared with accurate analytical solutions, the improvements of the calculation complication and the computation precision of asymptotic ones of $\mathrm{P_r}$ and $\bar{C}_S$ are +36.388%, -2.303%, +36.251%, and -2.365%, respectively. Based on the above statistics, improvements of the calculation complication are much greater than losses of the computation precision.

Herein, $Q_i = q_1\mathrm{ImTC}_{i,P_{\mathrm{r}}} + q_2\mathrm{ImTC}_{i,\bar{C}_S} + q_3\mathrm{ImTC}_{i,P_{\mathrm{r}}} + q_4\mathrm{ImCA}_{i,\bar{C}_S}, i \in \{1,2,3\}$, is defined as the evaluation function of the i^{th} case further, where $q_l, l \in \{1,2,3,4\}$ denotes the weight factor of the l^{th} parameter, and $\mathrm{ImTC}_{i,P_{\mathrm{r}}}$, $\mathrm{ImTC}_{i,\bar{C}_S}$, $\mathrm{ImTC}_{i,P_{\mathrm{r}}}$, and $\mathrm{ImCA}_{i,\bar{C}_S}$ represent improvements of $\mathrm{P_r}$ and $\bar{C}_S$ of time computation and computation accuracy in the Case i, respectively. Herein, four parameters q_1, q_2, q_3, and q_4 are all set as +25.000%. Therefore, in the Case 1, $Q_1 = 16.993\%$ indicates the comprehensive performance of the AA is superior to the conventional one.

2) From the Point of Vertical Direction: With H_s increasing, the calculation complexity get improved gradually, while the computation accuracy is affected negatively. However, this effect varies in a small and controllable range. Moreover, according to aforementioned discussions, the evaluation functions of three cases are given by $Q_1 = 16.993\%$, $Q_2 = 17.477\%$, and $Q_3 = 17.656\%$, respectively. The above statistics demonstrate that the AA can provide a considerable convenience for engineering applications.

Furthermore, to obtain a more clear comparison effect, all of values in TABLE II are normalized to be put in the

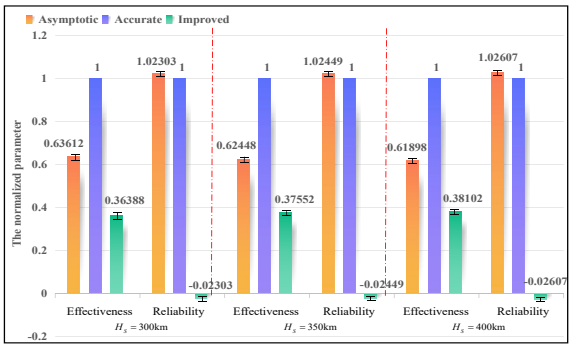

(a) Comparison of the specific performance improvement of $\mathrm{P_r}$.

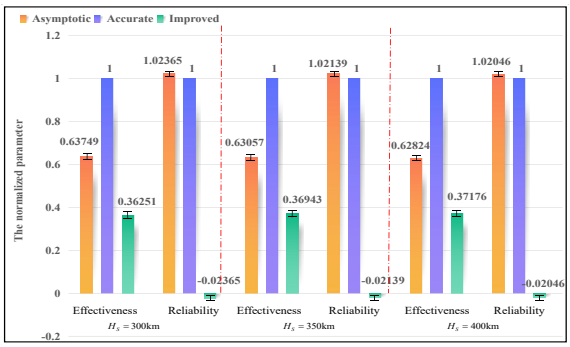

(b) Comparison of the specific performance improvement of $\bar{C}_S$.

Fig. 5: Comparison of the specific performance improvement of the STDT.

histogram, as is shown in Fig. 5. Then, the aforementioned differences analyzed are displayed intuitively in Fig. 5 further, where the abscissa and the ordinate represent the height of the satellite and the normalized parameter, respectively. As can be seen, Fig. 5(a) and Fig. 5(b) are divided into three zones, containing improvement comparisons between effectiveness and reliability at the corresponding height of the satellite of both $\mathrm{P_r}$ and $\bar{C}_S$. Herein, improvements on the calculated amount obtained is much more significant than the calculation precision lost. Owing to this remarkable advantage of the AA, its application in the engineering fields will be a more cost-effective and feasible alternative than conventional schemes.

VI. Conclusion

This paper sets out to investigate the SP of the satellite-terrestrial-vehicle network. Firstly, this thesis has provided a deeper sight into the randomness of terrestrial mobile terminals via the RGT utilized, based on which the statistical characteristics of the RSNR at terrestrial vehicles are given, and then the CFAEs of the SOP and the ESC are obtained. The second major finding was that the series form of gamma function has an excellent approximation effect for the lower incomplete gamma function in the high RSNR, which indicates that the asymptotic analysis can be regarded as an effective scheme to assess the SP of the system. Finally, the simulation analysis has also illustrated that the asymptotic solutions outperform the corresponding accurate results significantly in the effectiveness, and there exist optimal values for antenna numbers and fading parameter of the legitimate receiver for the enhancement of the effectiveness improvement.

Appendix A
Part of Derivations of the ESC

The accurate and aymptotic ESCs without containing the randomness of locations of terminals are expressed as Eq. (35) and Eq. (36), respectively

$$\bar{C}_{S|d_D,d_E} = \int_0^{\gamma_D} A_{35}B_{35}\mathrm{d}\gamma_D - \int_0^{\gamma_E} C_{35}D_{35}\mathrm{d}\gamma_E, \quad (35a)$$

$$A_{35} = F_{\Upsilon_E}(\gamma_E)\,|_0^{\gamma_E} d_D^{\tau}\frac{\tilde{\alpha}_D}{\tilde{\beta}_D}\log_2(1+\gamma_D)\,\theta_{Dk}, \quad (35b)$$

$$B_{35} = \sum_{k=0}^{\tilde{\varepsilon}_D - M_D} \exp(-\psi_D d_D^{\tau}\gamma_D)(d_D^{\tau}\gamma_D)^{k+M_D-1}, \quad (35c)$$

$$C_{35} = F_{\Upsilon_D}(\gamma_D)\,|_0^{\gamma_D} d_E^{\tau}\frac{\tilde{\alpha}_E}{\tilde{\beta}_E}\log_2(1+\gamma_E)\,\theta_{El}, \quad (35d)$$

$$D_{35} = \sum_{l=0}^{\tilde{\varepsilon}_E - M_E} \exp(-\psi_E d_E^{\tau}\gamma_E)(d_E^{\tau}\gamma_E)^{l+M_E-1}, \quad (35e)$$

$$\bar{C}^{\infty}_{S|d_D,d_E} = \int_0^{\gamma_D} A_{36}B_{36}\mathrm{d}\gamma_D - \int_0^{\gamma_E} C_{36}D_{36}\mathrm{d}\gamma_E, \quad (36a)$$

$$A_{36} = F^{\infty}_{\Upsilon_E}(\gamma_E)\,|_0^{\gamma_E}\frac{\tilde{\alpha}_D}{\tilde{\beta}_D}\theta_{Dk}\frac{(\psi_D d_D^{\tau})^{k+M_D}}{\psi_D^{k+M_D}}, \quad (36b)$$

$$B_{36} = {\gamma_D}^{k+M_D-1}\log_2(1+\gamma_D), \quad (36c)$$

$$C_{36} = F^{\infty}_{\Upsilon_D}(\gamma_D)\,|_0^{\gamma_D}\frac{\tilde{\alpha}_E}{\tilde{\beta}_E}\theta_{El}\frac{(\psi_E d_E^{\tau})^{l+M_E}}{\psi_E^{l+M_E}}, \quad (36d)$$

$$D_{36} = {\gamma_E}^{l+M_E-1}\log_2(1+\gamma_E). \quad (36e)$$

Then, by swapping the order of integration and sum, and adopting equations in [30], Eq. (35) and Eq. (36) can be rewritten as Eq. (37) and Eq. (38), respectively,

$$\bar{C}_{S|d_D,d_E} = \sum_{k=0}^{\tilde{\varepsilon}_D - M_D} A_{37}B_{37} - \sum_{l=0}^{\tilde{\varepsilon}_E - M_E} C_{37}D_{37}, \quad (37a)$$

$$A_{37} = F_{\Upsilon_E}(\gamma_E)\,|_0^{\gamma_E}\frac{\theta_{Dk}}{\ln 2}\frac{\tilde{\alpha}_D}{\tilde{\beta}_D}(d_D^{\tau})^{k+M_D}, \quad (37b)$$

$$B_{37} = \frac{\partial\left[(\psi_D d_D^{\tau})^{-v}\Gamma(v)\right]}{\partial v}\,|v = k+M_D\,, \quad (37c)$$

$$C_{37} = F_{\Upsilon_D}(\gamma_D)\,|_0^{\gamma_D}\frac{\theta_{El}}{\ln 2}\frac{\tilde{\alpha}_E}{\tilde{\beta}_E}(d_E^{\tau})^{l+M_E}, \quad (37d)$$

$$D_{37} = \frac{\partial\left[(\psi_E d_E^{\tau})^{-u}\Gamma(u)\right]}{\partial u}\,|u = l+M_E\,, \quad (37e)$$

and

$$\bar{C}_{S|d_D,d_E}^{\infty} = F_{\Upsilon_E}^{\infty}(\gamma_E)\,|_0^{\gamma_E}\frac{\tilde{\alpha}_D}{\tilde{\beta}_D\ln 2}\sum_{k=0}^{\tilde{\varepsilon}_D-M_D}\frac{\theta_{Dk}}{k+M_D}(A_{38}+B_{38}) - F_{\Upsilon_D}^{\infty}(\gamma_D)\,|_0^{\gamma_D}\frac{\tilde{\alpha}_E}{\tilde{\beta}_E\ln 2}\sum_{l=0}^{\tilde{\varepsilon}_E-M_E}\frac{\theta_{El}}{l+M_E}(C_{38}+D_{38}), \tag{38a}$$

$$A_{38} = (d_D^{\tau})^{k+M_D}\left({\gamma_D}^{k+M_D}-(-1)^{k+M_D}\right)\ln(1+\gamma_D), \tag{38b}$$

$$B_{38} = \sum_{p=1}^{k+M_D}\frac{(-1)^p{\gamma_D}^{k+M_D-p+1}}{k+M_D-p+1}, \tag{38c}$$

$$C_{38} = (d_E^{\tau})^{l+M_E}\left({\gamma_E}^{l+M_E}-(-1)^{l+M_E}\right)\ln(1+\gamma_E), \tag{38d}$$

$$D_{38} = \sum_{q=1}^{l+M_E}\frac{(-1)^q{\gamma_E}^{l+M_E-q+1}}{l+M_E-q+1}. \tag{38e}$$

Accordingly, the accurate CFAE with randomness of the ESC is given by

$$\bar{C}_S = \sum_{k=0}^{\tilde{\varepsilon}_D-A_D}\frac{\theta_{Dk}}{\ln 2}\frac{\tilde{\alpha}_D}{\tilde{\beta}_D}\psi_D^{-(k+A_D)}(A_{39}-B_{39}C_{39}) - \sum_{l=0}^{\tilde{\varepsilon}_E-A_E}\frac{\theta_{El}}{\ln 2}\frac{\tilde{\alpha}_E}{\tilde{\beta}_E}\psi_E^{-(l+A_E)}(D_{39}-E_{39}F_{39}), \tag{39a}$$

$$A_{39} = F_{\Upsilon_E}(\gamma_E)\,|_0^{\gamma_E}\frac{\partial\Gamma(v)}{\partial v}\,|v=k+A_D\,, \tag{39b}$$

$$B_{39} = F_{\Upsilon_E}(\gamma_E)\,|_0^{\gamma_E}\frac{\Gamma(k+A_D)}{L_s^2}, \tag{39c}$$

$$C_{39} = d_{\max}^2(\ln(\psi_D d_{\max}^{\tau})-1) - d_{\min}^2(\ln(\psi_D d_{\min}^{\tau})-1), \tag{39d}$$

$$D_{39} = F_{\Upsilon_D}(\gamma_D)\,|_0^{\gamma_D}\frac{\partial\Gamma(u)}{\partial u}\,|u=l+A_E\,, \tag{39e}$$

$$E_{39} = F_{\Upsilon_D}(\gamma_D)\,|_0^{\gamma_D}\frac{\Gamma(l+A_E)}{L_s^2}, \tag{39f}$$

$$F_{39} = d_{\max}^2(\ln(\psi_E d_{\max}^{\tau})-1) - d_{\min}^{\tau}(\ln(\psi_E d_{\min}^{\tau})-1). \tag{39g}$$

In a simialr way, the asymptotic CFAE is obtained as Eq. (40) and Eq. (41).

$$\bar{C}_S^{\infty} = F_{\Upsilon_E}^{\infty}(\gamma_E)\,|_0^{\gamma_E}\frac{\tilde{\alpha}_D}{\tilde{\beta}_D\ln 2}\sum_{k=0}^{\tilde{\varepsilon}_D-M_D}\theta_{Dk}(U_D V_D+W_D) - F_{\Upsilon_D}^{\infty}(\gamma_D)\,|_0^{\gamma_D}\frac{\tilde{\alpha}_E}{\tilde{\beta}_E\ln 2}\sum_{l=0}^{\tilde{\varepsilon}_E-M_E}\theta_{El}(U_E V_E+W_E), \tag{40a}$$

$$U_D = \frac{2\left({\gamma_D}^{k+M_D}-(-1)^{k+M_D}\right)\ln(1+\gamma_D)}{\tau L_s^2(k+M_D)}, \tag{40b}$$

$$V_D = \frac{(d_{\max}^{\tau})^{\frac{2}{\tau}+k+M_D}-(d_{\min}^{\tau})^{\frac{2}{\tau}+k+M_D}}{\frac{2}{\tau}+k+M_D}, \tag{41a}$$

$$W_D = \frac{\sum_{p=1}^{k+M_D}\frac{(-1)^p{\gamma_D}^{k+M_D-p+1}}{k+M_D-p+1}}{k+M_D}, \tag{41b}$$

$$U_E = \frac{2\left({\gamma_E}^{l+M_E}-(-1)^{l+M_E}\right)\ln(1+\gamma_E)}{\tau L_s^2(l+M_E)}, \tag{41c}$$

$$V_E = \frac{(d_{\max}^{\tau})^{\frac{2}{\tau}+l+M_E}-(d_{\min}^{\tau})^{\frac{2}{\tau}+l+M_E}}{\frac{2}{\tau}+l+M_E}, \tag{41d}$$

$$W_E = \frac{\sum_{q=1}^{l+M_E}\frac{(-1)^q{\gamma_E}^{l+M_E-q+1}}{l+M_E-q+1}}{l+M_E}. \tag{41e}$$

REFERENCES

[1] Shannon C. E., "Communication theory of secrecy systems," The Bell System Technical Journal, vol. 28, no. 4, pp. 656-715, Oct. 1949.

[2] Wyner A. D., "The wire-tap channel," The Bell System Technical Journal, vol. 54, no. 8, pp. 1355-1387, Oct. 1975.

[3] Leung Yan Cheong S and Hellman M, "The Gaussian wire-tap channel," *IEEE Trans. Inf. Theory*, vol. 16, no. 4, pp. 1670-1671, Dec. 2020.

[4] Kalantari, Ashkan and Zheng, Gan and Gao, Zhen and Han, Zhu and Ottersten Björn, "Secrecy analysis on network coding in bidirectional multibeam satellite communications," *IEEE Trans. Inf. Forensic Secur.*, vol. 10, no. 9, pp. 1862-1874, May. 2015.

[5] K. Guo, M. Lin, B. Zhang, J. Ouyang, and W. Zhu, "Secrecy performance of satellite wiretap channels with multi-user opportunistic scheduling," *IEEE Wirel. Commun. Lett.*, vol. 23, no. 11, pp. 2050-2051, Nov. 2019.

[6] W. Lu, K. An and T. Liang, "Robust beamforming design for sum secrecy rate maximization in multibeam satellite systems," *IEEE Trans. Aerosp. Electron. Syst.*, vol. 55, no. 3, pp. 1568-1572, June 2019.

[7] G. Cui, Q. Zhu, L. Xu and W. Wang, "Secure beamforming and jamming for multibeam satellite systems with correlated wiretap channels," *IEEE Trans. Veh. Technol.*, vol. 69, no. 10, pp. 12348-12353, Oct. 2020.

[8] Y. Fan, A. Li, X. Liao and V. C. M. Leung, "Secure interference exploitation precoding in MISO wiretap channel: destructive region redefinition with efficient solutions," *IEEE Trans. Inf. Forensic Secur.*, vol. 16, pp. 402-417, 2021.

[9] J. Du, C. Jiang, H. Zhang, X. Wang, Y. Ren and M. Debbah, "Secure satellite-terrestrial transmission over incumbent terrestrial networks via cooperative beamforming," *IEEE J. Sel. Areas Commun.*, vol. 36, no. 7, pp. 1367-1382, Jul. 2018.

[10] K. Guo, K. An, B. Zhang, Y. Huang, X. Tang, G. Zheng, and Theodoros A. Tsiftsis, "Physical layer security for multiuser satellite communication systems with threshold-based scheduling scheme," *IEEE Trans. Veh. Technol.*, vol. 69, no. 5, pp. 5129-5141, May. 2020.

[11] Y. Fan, R. Yao, A. Li, X. Liao and V. C. M. Leung, "Robust deception scheme for secure interference exploitation under PSK modulations," *IEEE Trans. Commun.*, vol. 69, no. 8, pp. 5425-5440, Aug. 2021.

[12] Z. Lin, M. Lin, J. Wang, Y. Huang and W. Zhu, "Robust secure beamforming for 5G cellular networks coexisting with satellite networks," *IEEE J. Sel. Areas Commun.*, vol. 36, no. 4, pp. 932-945, Apr. 2018.

[13] Z. Lin, M. Lin, J. Ouyang, W. Zhu, A. D. Panagopoulos and M. Alouini, "Robust secure beamforming for multibeam satellite communication systems," *IEEE Trans. Veh. Technol.*, vol. 68, no. 6, pp. 6202-6206, Jun. 2019.

[14] H. M. Tran, D. T. Le, B. C. Nguyen, N. X. Tran and T. Kim, "Secrecy outage performance of FD-NOMA relay system with multiple non-colluding eavesdroppers," *IEEE Trans. Veh. Technol.*, vol. 1, no. 1, pp. 1-13, Oct. 2021.

[15] Y. Yan, W. Yang, D. Guo, S. Li, H. Niu and B. Zhang, "Robust secure beamforming and power splitting for millimeter-wave cognitive satellite–terrestrial networks with SWIPT," *IEEE Syst. J.*, vol. 14, no. 3, pp. 3233-3244, Sep. 2020.

[16] Z. Yin, M. Jia, W. Wang, N. Cheng, F. Lyu, Q. Guo, and X. Shen, "Secrecy rate analysis of satellite communications with frequency domain NOMA," *IEEE Trans. Veh. Technol.*, vol. 68, no. 12, pp. 11847-11858, Dec. 2019.
[17] R. Xu, X. Da, H. Hu, L. Ni and Y. Pan, "Self-interference cancellation scheme for secure AF satellite communication based on FH-MWFRFT," *IEEE Commun. Lett.*, vol. 23, no. 11, pp. 2050-2053, Nov. 2019.
[18] M. G. Schraml, R. T. Schwarz, and A. Knopp, "Multiuser MIMO Concept for Physical Layer Security in Multibeam Satellite Systems," *IEEE Trans. Inf. Forensic Secur.*, vol. 16, pp. 1670-1680, Nov. 2021.
[19] J. Xiong, D. Ma, H. Zhao and F. Gu, "Secure multicast communications in cognitive satellite-terrestrial networks," *IEEE Commun. Lett.*, vol. 23, no. 4, pp. 632-635, Apr. 2019.
[20] Á. Vázquez-Castro and M. Hayashi, "Physical layer security for RF satellite channels in the finite-length regime," *IEEE Trans. Inf. Forensic Secur.*, vol. 14, no. 4, pp. 981-993, Apr. 2019.
[21] Oltjon Kodheli, Eva Lagunas, and Eicola Maturo, "Satellite communications in the new space era: a survey and future challenges," *IEEE Commun. Surv. Tutor.*, vol. 23, no. 1, pp. 70-71, Feb. 2021.
[22] J. Li, S. Han, and X. Tai, "Physical layer security enhancement for satellite communication among similar channels: relay selection and power allocation," *IEEE Syst. J.*, vol. 14, no. 1, pp. 433-444, Mar. 2020.
[23] M. Lin, Z. Lin, W. Zhu and J. Wang, "Joint beamforming for secure communication in cognitive satellite terrestrial networks," *IEEE J. Sel. Areas Commun.*, vol. 36, no. 5, pp. 1017-1029, May. 2018.
[24] K. An, M. Lin, J. Ouyang and W. Zhu, "Secure transmission in cognitive satellite terrestrial networks," *IEEE J. Sel. Areas Commun.*, vol. 34, no. 11, pp. 3025-3037, Nov. 2016.
[25] V. Bankey, and P. K. Upadhyay, "Physical layer security of multiuser multirelay hybrid satellite-terrestrial relay networks," *IEEE Trans. Veh. Technol.*, vol. 68, no. 3, pp. 2488-2501, Mar. 2019.
[26] L. Qian, P. Yang, Y. Guan, Z. Liu, Y. Xiao, K. Jiang, and M. Xiao, "Multi-dimensional polarized modulation for land mobile satellite communications," *IEEE Trans. Cogn. Commun. Netw.*, vol. 7, no. 2, pp. 383-397, Jun. 2021.
[27] Q. Huang, M. Lin, W.-P. Zhu, S. Chatzinotas and M.-S. Alouini, "Performance analysis of integrated satellite-terrestrial multiantenna relay networks with multiuser scheduling," *IEEE Trans. Aerosp. Electron. Syst.*, vol. 56, no. 4, pp. 2718-2731, Aug. 2020.
[28] G. Pan, J. Ye, and Z. Ding, "On secure VLC systems with spatially random terminals," *IEEE Commun. Lett.*, vol. 21, no. 3, pp. 492-494, Mar. 2017.
[29] M. Abramowitz and I. A. Stegun, *Handbook of Mathematical Functions with Formulas, Graphs, and Mathematical Tables*, 10th ed. New York: Dover, 1972.
[30] I. S. Gradshteyn and I. M. Ryzhik, *Table of Integrals, Series, and Products*, 7th ed. San Diego: Academic Press, 2007.
[31] L. Samara, R. Hamila, and N. Al-Dhahir, "Secrecy performance of full-duplex jamming and reception under I/Q imbalance," *IEEE Trans. Veh. Technol.*, vol. 70, no. 9, pp. 9560-9565, Sep. 2021.